Model-Agnostic Meta-Learning for Adaptive Gait Phase and Terrain Geometry Estimation With Wearable Soft Sensors

Zenan Zhu, Wenxi Chen, Pei-Chun Kao, Janelle Clark, *Member, IEEE*, Lily Behnke, Rebecca Kramer-Bottiglio, Holly Yanco, and Yan Gu

***Abstract*—This letter presents a model-agnostic meta-learning (MAML) based framework for simultaneous and accurate estimation of human gait phase and terrain geometry using a small set of fabric-based wearable soft sensors, with efficient adaptation to unseen subjects and strong generalization across different subjects and terrains. Inter-subject and inter-terrain variability, coupled with limited calibration data in real-world deployments, complicate accurate gait estimations. Further nonlinearities arise from fabric-based soft sensors, which improve comfort but introduce hysteresis, placement error, and fabric deformation. To address these challenges, the proposed framework integrates MAML into a deep learning architecture to learn a generalizable model initialization that captures subject- and terrain-invariant structure. This enables efficient adaptation to new users with a small amount of calibration data, while maintaining high estimation accuracy across subjects and terrains. Experiments on nine participants walking at various speeds over five terrain conditions demonstrate that the proposed framework outperforms baseline approaches in estimating gait phase, locomotion mode, and incline angle, with superior accuracy, adaptation efficiency, and generalization.**

***Index Terms*—Deep learning methods, prosthetics and exoskeletons, soft sensors, gait phase estimation, terrain estimation.**

Received 23 August 2025; accepted 4 February 2026. Date of publication 19 March 2026; date of current version 30 March 2026. This article was recommended for publication by Associate Editor Z. Guo and Editor H. Yu upon evaluation of the reviewers' comments. This work was supported by NSF under Grant IIS-1955979, Grant IIS-1954591, Grant CRA-203085, and Grant CRA-2127309. *(Zenan Zhu and Wenxi Chen contributed equally to this work.) (Corresponding author: Yan Gu.)*

This work involved human subjects or animals in its research. Approval of all ethical and experimental procedures and protocols was granted by the Purdue University IRB under Application No. 20-057-YAN-XPD.

Zenan Zhu, Wenxi Chen, and Yan Gu are with the School of Mechanical Engineering, Purdue University, West Lafayette, IN 47907 USA (e-mail: zhu1134@purdue.edu; chen4803@purdue.edu; yangu@purdue.edu).

Pei-Chun Kao is with the Department of Physical Therapy and Kinesiology, University of Massachusetts Lowell, Lowell, MA 01854 USA (e-mail: PeiChun_Kao@uml.edu).

Janelle Clark is with the Department of Mechanical Engineering, University of Maryland Baltimore County, Baltimore, MD 21250 USA (e-mail: janelle.clark@umbc.edu).

Lily Behnke and Rebecca Kramer-Bottiglio are with the Department of Mechanical Engineering & Materials Science, Yale University, New Haven, CT 06520 USA (e-mail: lily.behnke@yale.edu; rebecca.kramer@yale.edu).

Holly Yanco is with the Department of Mechanical & Industrial Engineering, Manning College of Information & Computer Sciences, University of Massachusetts Amherst, Amherst, MA 01003 USA (e-mail: holly@cs.uml.edu).

Digital Object Identifier 10.1109/LRA.2026.3675944

I. Introduction

ACCURATE estimation of human movement and terrain geometry can support lower-limb wearable robots (e.g., exoskeletons) to provide adaptive assistance under diverse conditions [1], [2]. Gait phase estimation allows synchronization of robot control with biomechanical events such as ankle push-off [3], [4], [5], while terrain estimation (e.g., incline angle estimation) can benefit smooth transitions across terrains [6].

In real-world deployment, estimators must adapt rapidly to previously unseen users with only a small amount of subject-specific calibration data, while maintaining high estimation accuracy across different users and terrain conditions. This poses substantial challenges for conventional learning methods, which typically rely on large training datasets and can experience performance degradation under subject- or terrain-specific variability [7].

A. Related Work

Recent studies have explored different sensing modalities, physics-based models, and learning methods to enable accurate estimation of human movement and terrain geometry.

1) Model-Based Estimation: To achieve real-time movement estimation, model-based methods commonly employ kinematic models and sensor fusion, such as dead-reckoning with foot-mounted inertial measurement units (IMUs) [8] and Kalman filters with biomechanical models [9]. Yet, their accuracy can be adversely affected by integration error accumulation, sensitivity to modeling assumptions, and uncertain limb geometry and sensor placement [10].

2) Learning-Based Estimation: Machine learning methods have been widely adopted for human movement estimation and to address nonlinearities of wearable soft sensors [11], [12], [13]. Yet, wearable systems that are fully tailored to a new user still require extensive recalibration data and fine-tuning [14]. This is due to substantial variations in individual gait patterns, influenced by factors such as age, muscle strength, and neuromuscular control [15], [16]. Transfer learning can reduce data requirements by pre-training on able-bodied subjects and selectively fine-tuning for unseen users (e.g., amputees) [17]; still, adaptation efficiency and generalization across unseen subjects may not be ensured due to distribution shift between training and test data.

3) Meta-Learning: Compared to conventional learning-based estimation methods, meta-learning follows the "model-agnostic" formulation, rendering it applicable to any differentiable neural network model regardless of architectural choices. As subjects and terrains tend to have high variability for gait tasks, this meta-learning framework's capacity for efficient task adaptation is particularly well-suited for the user-specific calibration required by wearable devices. [18]. Recent studies have demonstrated meta-learning's effectiveness for wearable sensing, including gait phase estimation from IMU data using stacked denoising autoencoders [19] and electromyography-based hand orthosis control [20]. Yet, these methods are typically evaluated in limited scenarios, e.g., a few movement modes and a single environment, leaving open questions about their generalizability to diverse subjects, movement patterns, and terrain conditions.

4) Rigid Vs. Soft Wearable Sensors: Prior methods of human movement and terrain geometry estimation often use rigid sensors such as IMUs and motion-capture systems [21], [22], which may be uncomfortable or impractical for continuous use. In contrast, soft sensors are lightweight, compliant, and garment-integrable, making them suitable for daily monitoring [23]. While most soft sensors in the literature and on the market are elastomer-based, recent fabric-based stretchable strain sensors offer enhanced comfort with improved air permeability and water vapor transmission [24]. Yet, these sensors exhibit inherent nonlinearities due to material properties, skin-garment shifts, and deformation from prolonged wear [25], [26], complicating accurate estimation.

B. Contributions

This study introduces a MAML-based estimation framework using a small set (i.e., four) of wearable soft sensors to accurately and simultaneously estimate human gait phase and terrain geometry. The main contributions are as follows: **(a)** Construction of a deep convolutional neural network (DCNN) with multi-head structure to simultaneously estimate gait phase, locomotion mode, and incline angle from a small amount of fabric-based sensor data. **(b)** Integration of MAML into the DCNN to enable rapid, data-efficient adaptation to unseen subjects and robust generalization across users and terrains. **(c)** Extensive evaluation on nine participants walking at multiple speeds and terrain types, demonstrating that the proposed approach outperforms standard supervised and transfer learning baselines in accuracy, adaptation efficiency, and generalization.

II. Problem Formulation

This section introduces the problem formulation for gait phase and terrain geometry estimation using soft sensor data.

A. Gait Phase and Terrain Geometry Definition

The problem formulation begins by defining the gait phase and terrain geometry variables to be estimated.

1) Gait Phase: A complete human walking cycle consists of four phases, each defined by distinct foot-ground contact conditions [27], as illustrated in Fig. 1. Accurate identification of these gait phases provides the temporal structure required for synchronizing wearable-robot assistance with human biomechanics, such as triggering ankle push-off torque during appropriate double-support intervals [28].

These phases, denoted as G1-G4, are: **G1** is a double-support phase with both feet on the ground and the right foot about to lift off; **G2** is a left-foot-single-support phase, with the left foot in contact and the right foot swinging; **G3** is another double-support phase with the left foot about to lift off; and **G4** is a right-foot-single-support phase, with only the right foot in contact.

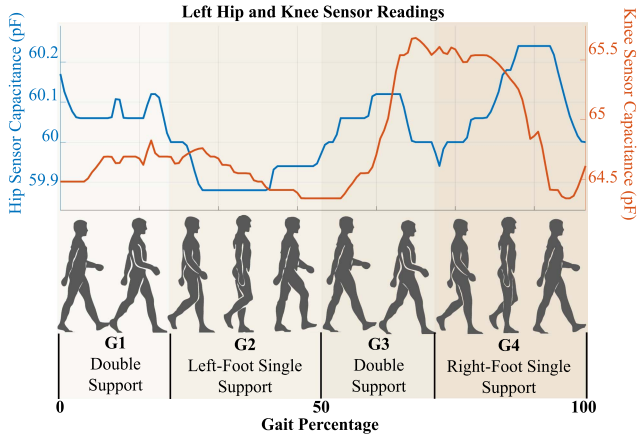

Fig. 1. Example of walking gait phases along with representative soft sensor measurements.

2) Terrain Geometry: To reflect common real-world terrains, we classify five discrete locomotion modes: **level walking (LW)**, **ramp ascent (RA)**, **ramp descent (RD)**, **stair ascent (SA)**, and **stair descent (SD)**. Also, we estimate the terrain slope angle. Recognizing terrain geometry enables an exoskeleton controller to adapt assistance to environment demands (e.g., increasing torque during stair ascent).

3) Estimation Variables: This study focuses on estimating three variables at each time step $t \in \mathbb{N}_+$: gait phase $g_t \in \{\text{G1, G2, G3, G4}\}$, locomotion mode $l_t \in \{\text{LW, RA, RD, SA, SD}\}$, and terrain incline angle $\phi_t \in \mathbb{R}$. Here, $(\cdot)_t$ denotes the value of the variable $(\cdot)$ at time t. Note that the locomotion mode l_t and gait phase g_t are discrete variables with symbolic labels, while the incline angle ϕ_t is treated as a continuous variable.

B. Sensors Considered

To enhance wearer comfort compared to rigid sensors, this study uses data from a small set of (i.e., four) fabric sensors [24] embedded in compression pants and placed along the sagittal planes at the hip and knee joints (Fig. 3(C)). Adopting the five-layer shielded configuration, each sensor comprises two dielectric layers (with one formed by the pants) and three electrode layers, all made of nylon, where the external electrode is grounded to minimize environmental interference. Due to humidity and sweat sensitivity, the sensors are encapsulated in elastomer. The encapsulated sensors are embedded in the garment, with the garment itself acting as one of the dielectric layers in the capacitor, such that they remain stretched during quiet standing. As a hip or knee rotates, the corresponding sensor stretches, producing capacitance changes that reflect joint angle variations (Fig. 1).

C. Objective

This study aims to achieve accurate and simultaneous estimation of gait phase g_t, locomotion mode l_t, and terrain incline angle ϕ_t using only a small set of wearable soft sensors, with efficient adaptation (i.e., rapid fine-tuning to unseen users using

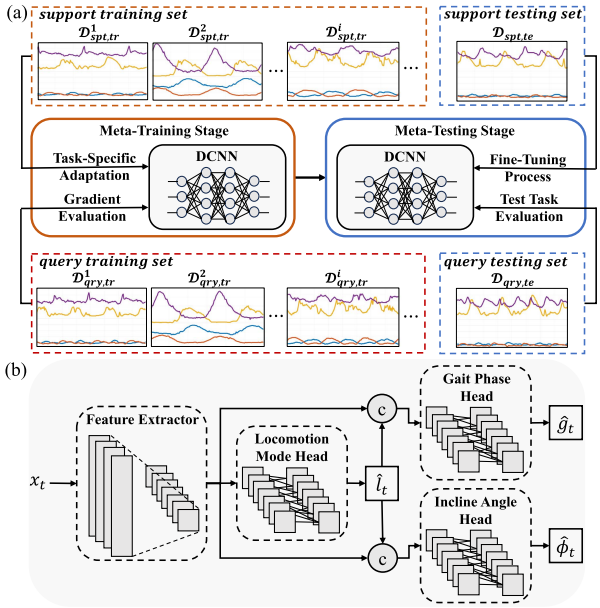

Fig. 2. (a) MAML pipeline with task-specific adaptation and gradient aggregation during meta-training. (b) DCNN model shared by meta-training and meta-testing.

limited calibration data) and high generalization (i.e., consistently accurate estimation across locomotion modes and terrain geometry after efficient adaptation to unseen subjects). A key challenge lies in the substantial variability across individuals and terrains, due to differences in sensor placement, movement patterns, terrain characteristics, and the inherent nonlinearities of soft sensors.

III. Methodology

This section presents the proposed MAML-based framework for estimating gait phase and terrain geometry. To jointly estimate gait phase and terrain geometry over time, we choose to construct a DCNN (Fig. 2(B)) as the backbone of the proposed framework, considering its ability to capture local temporal patterns in time-series data and support multi-output estimation. Soft sensor nonlinearity causes complex dependency of capacitance not only on strain, but also on deformation frequency and loading cycles [24]. For instance, hysteresis can cause 20% signal deviations for a single joint angle depending on motion history. If uncompensated, this ambiguity creates joint angle measurement inaccuracy of 10°–15°. The proposed DCNN could implicitly address this by extracting temporal features from the sensor history, allowing the model to distinguish human subjects' kinematic information from these material-inherent nonlinearities.

Further, the proposed framework incorporates an MAML pipeline that comprises two stages (Fig. 2(A)): meta-training and meta-testing, with meta-training the key to efficient adaptation and strong generalization. During meta-training, the DCNN model learns a generalizable initialization by performing task-specific adaptation and aggregating gradients across different subjects and terrains. Meta-testing involves deploying the meta-trained DCNN on unseen users, using limited calibration data for rapid fine-tuning.

Algorithm 1: Meta-Training of the Proposed MAML-Based State Estimation Approach.

Require: Data partitioned by training tasks $\mathcal{T}_{\text{tr}}^i$
Require: α, β: step size hyperparameters
Randomly initialize θ
while not converged **do**
  for all $\mathcal{T}_{\text{tr}}^i$ **do**
    Sample training set $\mathcal{D}_{\text{tr}}^i \sim \mathcal{T}_{\text{tr}}^i$ and partition into disjoint support set $\mathcal{D}_{\text{spt,tr}}^i$ and query set $\mathcal{D}_{\text{qry,tr}}^i$
    Evaluate gradient of loss on support set $\nabla_\theta \mathcal{L}(f_\theta; \mathcal{D}_{\text{spt,tr}}^i)$
    Compute adapted parameters with gradient descent: $\theta_i' = \theta - \alpha \nabla_\theta \mathcal{L}(f_\theta; \mathcal{D}_{\text{spt,tr}}^i)$
    Evaluate loss on query set with adapted parameters $\mathcal{L}(f_{\theta_i'}; \mathcal{D}_{\text{qry,tr}}^i)$
  end for
  Update $\theta \leftarrow \theta - \beta \nabla_\theta \sum_i \mathcal{L}(f_{\theta_i'}; \mathcal{D}_{\text{qry,tr}}^i)$
end while

A. DCNN Model

For joint estimation of gait phase and terrain geometry, the DCNN employs a multi-head architecture (Fig. 2(B)):

1) Multi-Head Structure: The DCNN includes three heads: (a) a locomotion mode classification head for l_t; (b) a gait phase classification head for g_t; and (c) an incline regression angle head for ϕ_t. Each head is a two-layer perceptron with ReLU activation. To reduce computational overhead, all three heads share the same extracted features.

A distinguishing feature of the multi-head design is that the predicted locomotion mode is concatenated with the shared features and used as input to the gait phase and incline angle heads. This reflects the biomechanical dependency of the estimated variables (e.g., locomotion mode affects joint kinematics).

2) Model Input: To allow estimation with only a few soft sensors, we construct the model input at each time step $t \in \mathbb{N}_+$ from a sliding window of the previous k frames from four sensor channels at the hips and knees (Section II-B). Formally, the input $x_t \in \mathbb{R}^{4\times k}$ captures short-term motion characteristics. In our experiments (Section IV), we use $k = 100$ (approx. one second), which typically spans a full gait cycle.

3) Model Output: Since the proposed framework aims to estimate gait phase g_t, locomotion mode l_t, and terrain incline angle ϕ_t at each time step t (Section II-A3), we define the DCNN model's output as $y_t := \{l_t, g_t, \phi_t\}$. Given input x_t, the DCNN model, parameterized by θ and denoted as f_θ, predicts an estimate $\hat{y}_t$ of the output, i.e., $\hat{y}_t = f_\theta(x_t)$.

4) Feature Extractor: To ensure efficiency and prevent overfitting, a feature extractor is constructed with a one-dimensional convolutional layer for processing the temporal input signal x_t, followed by a batch normalization layer and a rectified linear unit (ReLU) activation function.

B. Meta-Training Stage

The meta-training stage learns a DCNN model initialization that can enable efficient adaptation to new conditions and strong generalization across deployment conditions.

1) Algorithm Overview: As summarized in Algorithm 1, we partition the training data by different *tasks*. Each task $\mathcal{T}_{\text{tr}}^i$ corresponds to a walking session by a subject under a specific terrain condition and speed. This construction formulates a

Fig. 3. Experimental setup: (a) Out-of-lab stair trials; (b) in-lab inclined treadmill walking; and (c) soft sensors at hips and knees, along with ExoBoots ankle exoskeletons used solely for ground-truth labeling during stair trials.

meta-learning problem: tasks share underlying biomechanical structure (e.g., gait phase sequences) yet exhibit distinct feature distributions due to subject kinematics and terrain differences. This encourages the model to learn an initialization that captures the shared structure while remaining adaptable to the unique distributions of unseen deployment scenarios.

Within each meta-training epoch (i.e., a single iteration of the `while` loop), two main steps are performed for each task: (I) **task-specific adaptation**, where the model is fine-tuned on each task's support set to obtain task-adapted parameters θ_i', and (II) **meta-update**, where the shared initialization θ is updated based on query set losses aggregated across tasks.

2) Loss Function Design: Meta-training uses a loss function $\mathcal{L}$, which we define as the weighted sum of the estimation errors of the gait phase, incline angle, and locomotion mode. The loss of model f_θ evaluated on a dataset $\mathcal{D}$ is:

$$\begin{aligned}&\mathcal{L}\left(f_\theta;\mathcal{D}\right)\\&=w_{\text{gait}}\,\mathcal{L}_{\text{gait}}\left(f_\theta;\mathcal{D}\right)+w_{\text{inc}}\,\mathcal{L}_{\text{inc}}\left(f_\theta;\mathcal{D}\right)+w_{\text{loc}}\,\mathcal{L}_{\text{loc}}\left(f_\theta;\mathcal{D}\right),\end{aligned}\tag{1}$$

where w_{gait}, w_{inc}, and w_{loc} are predefined weighting factors, and $\mathcal{L}_{\text{gait}}$, $\mathcal{L}_{\text{inc}}$, and $\mathcal{L}_{\text{loc}}$ denote individual task losses.

For the classification of locomotion mode and gait phase and the regression associated with incline angle estimation, we choose the commonly used cross-entropy loss and root-mean-square error (RMSE), respectively. The same loss functions and weighting parameters are applied for both meta-training and meta-testing, including fine-tuning steps.

3) Sampling Support and Query Sets (Line 4 of Algorithm 1): At each `for` loop iteration, a training dataset $\mathcal{D}_{\text{tr}}^i$ is sampled from the training task $\mathcal{T}_{\text{tr}}^i$. As illustrated in Fig. 2(A), this dataset is partitioned into a support set $\mathcal{D}_{\text{spt,tr}}^i=\{(x_j,y_j)\}_{j=1}^n$ and a query set $\mathcal{D}_{\text{qry,tr}}^i=\{(x_j,y_j)\}_{j=1}^m$, where n and m are the dataset sizes.

4) Task-Specific Adaptation With Support Sets (Lines 5 and 6 in Algorithm 1): The purpose of task-specific adaptation is to simulate deployment-time fine-tuning, where the model must quickly specialize to new settings using only a small amount of calibration data.

Given a model f_θ and a task-specific support set $\mathcal{D}_{\text{spt,tr}}^i$, the model parameters are adapted using gradient descent:

$$\theta_i'=\theta-\alpha\,\nabla_\theta\,\mathcal{L}\left(f_\theta;\mathcal{D}_{\text{spt,tr}}^i\right),\tag{2}$$

where α is a task-agnostic learning rate selected via hyperparameter tuning.

5) Meta-Update Step Using Query Sets (Lines 7 and 9 of Algorithm 1): The meta-update step begins by computing the gradient of the loss for the adapted model $f_{\theta_i'}$ on its query set $\mathcal{D}_{\text{qry,tr}}^i$. The gradients $\nabla_\theta\mathcal{L}(f_{\theta_i'},\mathcal{D}_{\text{qry,tr}}^i)$ are aggregated across all tasks to update θ as:

$$\theta\leftarrow\theta-\beta\nabla_\theta\sum_i\mathcal{L}\left(f_{\theta_i'};\mathcal{D}_{\text{qry,tr}}^i\right),\tag{3}$$

with β a learning rate selected via hyperparameter tuning. Meta-update captures MAML's core idea: aggregating gradients across diverse tasks to improve the model initialization θ. This preserves task-level variability during training, supporting rapid adaptation to unseen tasks with limited calibration data during deployment. In contrast, standard optimization methods such as stochastic gradient descent (SGD) update model parameters using gradients from mini-batches drawn from the overall data distribution, which may overlook task-specific structure and limit adaptation to unseen settings.

C. Meta-Testing Stage

Meta-testing evaluates the trained model's ability to adapt to an unseen task $\mathcal{T}_{\text{te}}$, which may differ from training tasks due to distribution shift. Note that for clarity and without loss of generality, this study focuses on a single test task.

In practice, the meta-testing stage fine-tunes the pre-trained model on a new task $\mathcal{T}_{\text{te}}$. The calibration process requires a small set of support data (also known as calibration data), which is used with a general optimization algorithm such as SGD to update the model parameters θ. The model is then evaluated on the test task $\mathcal{T}_{\text{te}}$.

IV. Experiments

This section reports the experimental validation results, including comparison with various baseline approaches.

A. Experimental Setup

1) Hardware: The hardware setup includes an instrumented Motek M-Gait treadmill (Fig. 3(B)) for configurable in-lab walking experiments and indoor stairs (Fig. 3(A)) for out-of-lab trials. In all experiments, subjects wore compression pants with four encapsulated fabric sensors [24] embedded, as described in Section II, as well as a pair of Dephy ExoBoot ankle exoskeletons (Fig. 3(C)). For stair trials, the exoskeleton data is used for ground-truth gait phase labeling. Although exoskeleton data was not needed for treadmill trials as the treadmill's force plates can support ground-truth gait phase labeling (Section IV-A5), subjects still wore the exoskeletons for maintaining consistent sensor placement and experimental conditions across treadmill and stair trials. Model training and testing were conducted on

a workstation with an Intel 14900 K CPU and an Nvidia RTX 4090 GPU.

2) Subjects: To assess subject-level generalizability, data were collected from nine participants (7 males, 2 females; 25 ± 4 yr. old; 1.70 ± 0.11 m tall; 60 ± 16 kg) under Purdue University IRB approval (20-057-YAN-XPD).

3) Terrains and Walking Speeds: For evaluation across different terrain types, walking experiments were conducted on a treadmill and a staircase (Fig. 3(A,B)).

Treadmill trials included **level walking (LW)**, **ramp ascent (RA)**, and **ramp descent (RD)** at incline angles of $0°$, $\pm 5°$, and $\pm 10°$. Walking speeds were 0.9, 1.1, and 1.3 m/s for LW, and 0.7, 0.9, and 1.1 m/s for RA and RD. Each subject completed two 2-minute treadmill trials per angle-speed combination in a fixed order, with all trials conducted on the same day to maintain consistency across participants. **Stair ascent (SA)** and **stair descent (SD)** trials were conducted on a staircase with 18 cm-high and 28 cm-deep steps (approx. $33°$ slope). Participants climbed 12 steps at self-selected speeds (approx. 0.8-1.0 m/s), completing five 10-second trials on a separate day from treadmill trials to ensure consistent performance.

4) Data Acquisition: Raw capacitance signals from the soft sensors are acquired via an Arduino board and logged by an Nvidia Jetson Orin Nano. The boards are carried in a fanny pack worn on the user's lower back (Fig. 3(C)).

5) Ground-Truth Labeling: Gait phases during treadmill trials are labeled using ground reaction forces, which are measured by the treadmill's force plates at 1000 Hz with a 5 mm center-of-pressure error. For stair trials, a finite-state machine (FSM) identifies the boundaries between gait phases by detecting heel-strike and toe-off events from ExoBoots' accelerometer signals. The FSM thresholds are calibrated against treadmill force plate data. Ground-truth locomotion modes are labeled based on the experimental protocol, while the ground-truth incline angles are obtained through direct geometry measurement for stair trials and incline pre-programming for treadmill experiments.

B. Baseline Setup

We compare the proposed MAML-based estimation framework against baseline learning approaches of increasing complexity to systematically evaluate adaptation efficiency and generalization across subjects and terrains. For both the proposed and baseline approaches, the entire dataset is partitioned with eight subjects for training (if any) and one held-out subject for testing (deployment).

1) Baseline Approaches: All baselines adopt the same DCNN architecture and weighted loss function as the proposed framework, with identical weights w_{gait}, w_{inc}, and w_{loc}.

We evaluate the following baselines commonly used in meta-learning studies [20], [29] and in transfer-learning-based gait phase estimation [17]: **(i) Random initialization (RI): no pre-training.** The DCNN model is trained from scratch on the support set of the unseen subject using randomly initialized parameters, without any pre-training on the other subjects. **(ii) Direct evaluation (DE): pre-training + no fine-tuning.** The model is pre-trained on data from eight subjects and evaluated on the unseen subject without any parameter fine-tuning. **(iii) Transfer learning (TL): pre-training + partially freezing fine-tuning.** Following [17], the model is pre-trained on eight subjects, and then fine-tuned on the unseen subject by updating only the model's top layers while earlier convolutional layers are frozen. **(iv) Standard fine-tuning (SFT): pre-training + full fine-tuning.** The model is pre-trained on the eight-subject dataset, and all layers are fine-tuned on the unseen test subject, reflecting a standard full fine-tuning approach. Pre-training of DE, TL, and SFT is based on conventional supervised learning instead of the MAML pipeline.

C. Training Setup

1) Network Size: The proposed network consists of a one-dimensional convolutional layer followed by batch normalization, a ReLU activation, and fully connected layers with a hidden size of 512. The convolutional layer has 32 output channels, a kernel size of 40, a stride of 1, a dilation of 1, and no padding. Ablation results on network capacity (varying from 128 to 512 units) indicate that the chosen 512-unit configuration provides the optimal balance of model expressiveness and adaptation efficiency. Both baselines and MAML share the same neural network architecture and size.

2) Loss Function Weights: The same loss weights are used for both MAML and baselines during training and fine-tuning, with $w_{\text{gait}} = 0.6$ and $w_{\text{inc}} = w_{\text{loc}} = 0.2$. The locomotion mode loss is down-weighted due to its indirect optimization through gait and incline estimation, while the incline loss is reduced because its regression head converges quickly during training. We also tested equal loss weights ($w_{\text{gait}} = w_{\text{loc}} = w_{\text{inc}} = 0.33$), and found the gait phase estimation has a 1-2% accuracy drop after fine-tuning and other estimations' performance is roughly the same.

3) MAML Training: For meta-training, each task dataset is divided into an 80-sample support set and a 120-sample query set ($n = 80$ and $m = 120$) to balance adaptation and meta-update. Meta-training is performed for 200 epochs (each epoch iterates over all tasks in Algorithm 1) to ensure model parameter convergence.

4) Baseline Training: The baselines DE, TL, and SFT are trained using the Adam optimizer [30] with 200 data points per batch. Training is conducted on the combined dataset from eight subjects until convergence, using the same input-output format (x, y) as MAML. Since RI does not include pre-training, it is excluded from this process.

D. Testing Setup

1) Hyperparameter Selection for Fine-Tuning: To ensure fair comparison of fine-tuning performance, we apply Bayesian optimization [31] to select the optimal SGD learning rate for each method, aiming to maximize average prediction accuracy after fine-tuning. The selected learning rates are: 3×10^{-4} for MAML; 1.5×10^{-4} for RI; 8×10^{-4} for TL; and 1×10^{-6} for SFT. DE is excluded from this process, as it does not involve fine-tuning.

2) Evaluation Scenarios for Adaptation and Generalization: To evaluate each approach's adaptation to an unseen subject under varying calibration data sizes and fine-tuning steps (i.e., gradient update steps), as well as its generalization across subjects and locomotion modes after fine-tuning, we consider three scenarios: **(S1) Data efficiency of adaptation:** Fixing four fine-tuning steps, we vary calibration data duration (across 1.5, 2, 2.5, 3, and 3.5 s per locomotion mode and speed) to assess adaptation with brief data. **(S2) Computation efficiency of adaptation:** Fixing calibration data to 3.5 s, we vary the number of fine-tuning

TABLE I
SUBJECT-SPECIFIC ESTIMATION ACCURACY USING 3.5 S OF CALIBRATION DATA AND FOUR FINE-TUNING STEPS, I.E., UNDER SCENARIO (S3). VALUES SHOW MEAN ACCURACY (CLASSIFICATION) OR RMSE (INCLINE ANGLE) WITH A 95% CI. THE TABLE HIGHLIGHTS **THE BEST PERFORMANCE**, THE SECOND-BEST PERFORMANCE, AND PROPOSED METHOD.

	Method	Sub01	Sub02	Sub03	Sub04	Sub05	Sub06	Sub07	Sub08	Sub09	Average
Gait Phase Accuracy	MAML	**0.84±0.02**	0.86±0.02	0.85±0.03	**0.88±0.01**	**0.87±0.01**	0.84±0.02	**0.86±0.02**	**0.84±0.02**	**0.82±0.03**	**0.85±0.01**
	RI	0.36±0.03	0.34±0.04	0.36±0.03	0.35±0.04	0.36±0.04	0.35±0.05	0.39±0.04	0.35±0.03	0.36±0.04	0.36±0.01
	DE	0.75±0.06	0.85±0.02	0.79±0.05	0.78±0.03	0.81±0.02	0.79±0.03	0.80±0.03	0.78±0.03	0.68±0.07	0.78±0.02
	TL	0.83±0.03	**0.88±0.02**	**0.86±0.02**	0.86±0.02	0.85±0.01	**0.85±0.02**	0.85±0.02	0.83±0.02	0.80±0.03	0.84±0.01
	SFT	0.79±0.06	0.86±0.02	0.79±0.05	0.78±0.04	0.83±0.03	0.79±0.03	0.82±0.02	0.80±0.03	0.69±0.07	0.79±0.02
Loc. Mode Accuracy	MAML	**1.00±0.00**	**1.00±0.00**	**1.00±0.00**	**1.00±0.00**	**1.00±0.00**	**1.00±0.00**	**1.00±0.00**	**1.00±0.00**	**1.00±0.00**	**1.00±0.00**
	RI	**1.00±0.00**	**1.00±0.00**	**1.00±0.00**	0.96±0.01	0.96±0.08	**1.00±0.00**	**1.00±0.00**	**1.00±0.00**	**1.00±0.00**	0.99±0.01
	DE	0.75±0.14	0.83±0.11	0.72±0.15	0.80±0.07	0.81±0.08	0.80±0.09	0.91±0.03	0.76±0.07	0.38±0.14	0.75±0.04
	TL	0.91±0.07	0.88±0.08	0.83±0.11	0.91±0.04	0.87±0.06	0.90±0.06	0.95±0.02	0.89±0.05	0.65±0.10	0.87±0.03
	SFT	0.87±0.10	0.98±0.02	0.95±0.05	0.94±0.05	0.98±0.01	0.98±0.02	0.98±0.01	0.95±0.03	0.82±0.10	0.94±0.02
Incline RMSE (°)	MAML	2.75±0.30	2.57±0.22	2.51±0.15	**2.63±0.17**	2.69±0.20	**2.60±0.19**	**2.54±0.18**	2.79±0.28	2.98±0.41	**2.67±0.09**
	RI	3.56±0.40	3.67±0.48	3.89±0.41	3.73±0.38	3.60±0.27	3.81±0.51	3.81±0.50	3.53±0.36	3.77±0.40	3.71±0.14
	DE	7.52±3.35	5.19±1.29	9.18±1.92	13.94±4.73	6.97±1.83	11.66±3.61	9.94±3.48	7.82±2.05	12.26±3.68	9.51±1.11
	TL	3.74±1.69	2.57±0.72	3.10±0.55	3.46±0.74	2.86±0.49	3.95±1.13	4.10±1.49	3.36±0.67	3.54±0.83	3.42±0.34
	SFT	**2.40±0.65**	**1.89±0.34**	**2.47±0.39**	4.96±1.75	**2.60±0.62**	3.13±0.68	4.21±1.73	**2.46±0.40**	**2.63±0.47**	3.01±0.35

TABLE II
LOCOMOTION-MODE-SPECIFIC ESTIMATION ACCURACY USING 3.5 S OF CALIBRATION DATA AND FOUR FINE-TUNING STEPS, I.E., UNDER SCENARIO (S3). FORMATTING FOLLOWS TABLE I.

	Method	LW	RA	RD	SA	SD
Gait Phase Accuracy	MAML	**0.89±0.01**	0.85±0.01	**0.85±0.01**	**0.85±0.02**	**0.84±0.02**
	RI	0.40±0.01	0.38±0.01	0.40±0.00	0.28±0.03	0.32±0.03
	DE	0.87±0.02	0.82±0.02	0.82±0.02	0.73±0.04	0.66±0.04
	TL	0.88±0.01	0.85±0.01	0.84±0.01	**0.85±0.02**	0.81±0.02
	SFT	0.87±0.02	**0.86±0.01**	0.84±0.01	0.72±0.04	0.67±0.04
Loc. Mode Accuracy	MAML	**1.00±0.00**	**1.00±0.00**	**1.00±0.00**	**1.00±0.00**	**1.00±0.00**
	RI	**1.00±0.00**	**1.00±0.00**	**1.00±0.00**	0.97±0.05	**1.00±0.00**
	DE	0.49±0.11	0.95±0.02	0.62±0.08	0.76±0.09	0.82±0.09
	TL	0.70±0.08	0.97±0.01	0.76±0.05	0.88±0.06	0.97±0.02
	SFT	0.91±0.05	0.99±0.01	0.97±0.02	0.81±0.08	0.98±0.02
Incline RMSE (°)	MAML	2.18±0.05	2.32±0.05	2.31±0.04	**3.19±0.13**	**3.39±0.21**
	RI	3.45±0.31	3.61±0.22	3.73±0.24	4.24±0.26	4.14±0.25
	DE	3.89±0.61	3.55±0.38	5.64±0.66	17.79±2.06	18.47±2.61
	TL	2.12±0.17	1.89±0.11	2.37±0.15	6.03±1.05	5.09±0.70
	SFT	**1.54±0.11**	**1.51±0.07**	**1.83±0.08**	5.68±1.19	4.69±0.42

steps (0–4) to evaluate adaptation speed. **(S3) Generalizability across subjects and locomotion modes after fine-tuning:** With both calibration data (3.5 s) and fine-tuning steps (4) fixed, we compare estimation accuracy across individual subjects and locomotion modes to assess post-adaptation generalization.

3) Estimation Accuracy Measures: All evaluation results (e.g., Tables I and II) are aggregated across the multiple walking speeds collected for each terrain condition. Accuracy for gait phase and locomotion mode classification is computed as the total number of correct predictions divided by the total number of test query samples. Incline angle accuracy is evaluated using RMSE. All results are presented as mean ± 95% confidence interval (CI).

E. Result Analysis and Discussion

We compare the performance of all approaches as follows.

1) Comparison on Data Efficiency of Adaptation: Using the test results from Scenario (S1), we evaluate the calibration data efficiency of the proposed MAML-based estimation framework and baseline methods under varying calibration data sizes during deployment. Figure 4(A) presents the estimation accuracy of all algorithms with a fixed number of fine-tuning steps across the different calibration data sizes.

MAML achieves the highest calibration data efficiency in adaptation. As calibration data increases to 2 s and beyond, MAML consistently reaches the highest accuracy for all three estimation problems among all approaches. This confirms its ability to adapt effectively to unseen subjects using limited data. In comparison, TL and SFT require significantly more data to reach similar accuracy.

Pre-training is critical for accurate gait phase classification. RI underperforms significantly in gait phase classification compared to terrain geometry and locomotion mode estimation. This is likely due to the fine-grained, high-temporal-resolution features needed for phase estimation, which are difficult to learn from scratch with limited data. In contrast, locomotion mode classification involves more coarse-grained features and may be less sensitive to pre-training, explaining RI's stronger performance in locomotion mode classification compared to gait phase estimation.

Standard pre-training is not always superior to training from scratch, especially with sufficient task-specific calibration data. With sufficient calibration data (e.g., >2.5 s), RI surpasses all methods that rely on pre-training, except MAML, in locomotion mode classification. Also, RI achieves similar accuracy as TL and SFT in incline angle estimation. This suggests that with sufficient task-specific calibration data available, standard pre-training offers limited benefit for some estimation problems.

2) Comparison on Computation Efficiency of Adaptation: Figure 4(B) displays the estimation accuracy results under Scenario (S2) where the computational efficiency of fine-tuning is evaluated by using a fixed 3.5 s of calibration data and varying the number of fine-tuning steps from 0 to 4. The accuracy at zero fine-tuning steps reflects the zero-shot generalization capability of each method, and recall that SFT and TL without fine-tuning reduce to DE. Since DE involves no fine-tuning, its performance remains constant across all conditions and serves as the baseline for zero-shot accuracy.

MAML enables computationally efficient fine-tuning. Figure 4(B) shows that while MAML matches DE in gait phase classification at zero fine-tuning steps, it performs slightly worse in locomotion mode and incline angle estimation. However, with just one or two fine-tuning steps, MAML rapidly outperforms all baseline methods across all three estimation problems. This highlights MAML's strength in computational adaptation efficiency: instead of optimizing solely for zero-shot generalization, it learns model parameters that are highly adaptable to new conditions, enabling accurate estimation with minimal fine-tuning.

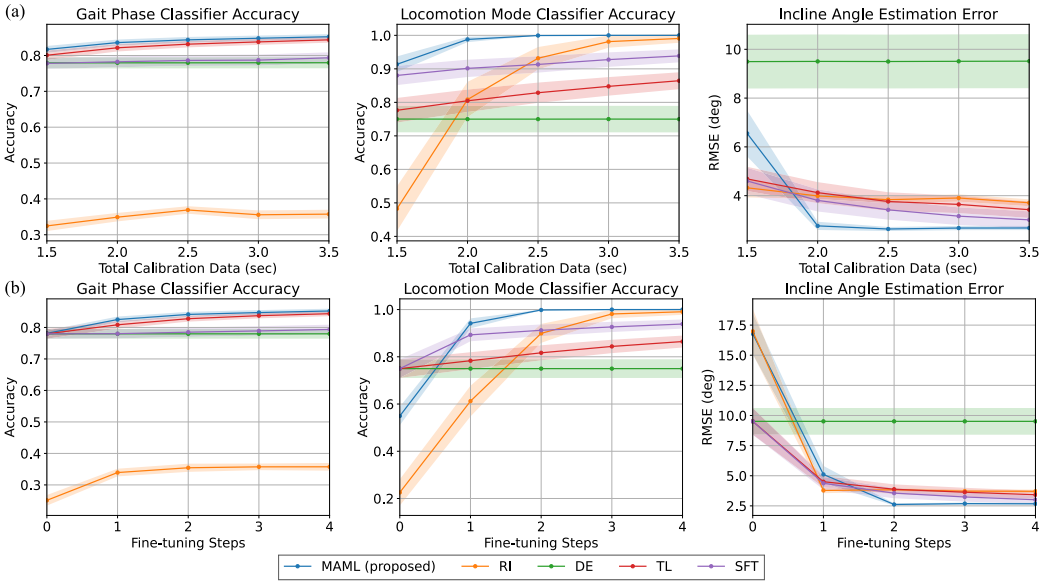

Fig. 4. (a) Effect of calibration data size on estimation accuracy with four fine-tuning steps (scenario S1). (b) Effect of fine-tuning steps on estimation accuracy using 3.5 s of calibration data (scenario S2). Solid lines and shaded areas denote mean and 95% CI across subjects.

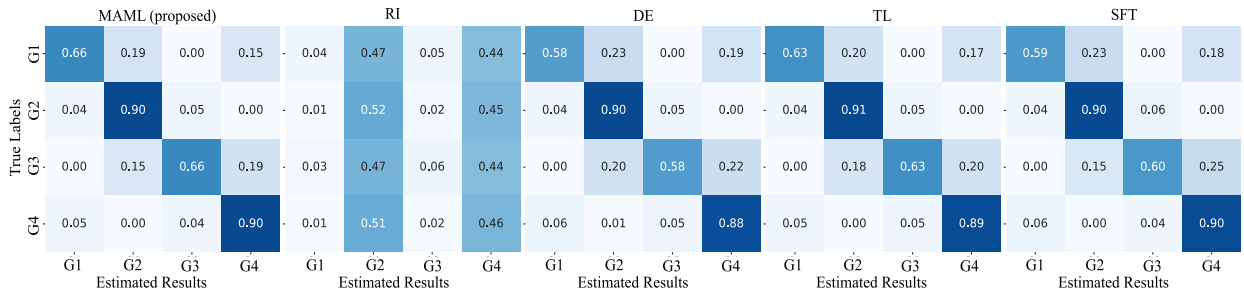

Fig. 5. Confusion matrices for gait phase classification using 3.5 s of calibration data and two fine-tuning steps (scenario S2). Darker diagonal cells indicate higher accuracy.

3) Analysis of Gait Phase Misclassification: To provide insights into gait phase classification, Fig. 5 shows the confusion matrices after two fine-tuning steps using 3.5 s of support data, which is a special case under Scenario (S2).

Most gait phase misclassifications tend to occur between adjacent phases across all methods, as reflected by the off-diagonal entries. These errors may be partially attributed to the inherent ambiguity near phase transitions, as well as the inevitable labeling inaccuracies caused by hardware imperfections (e.g., noise and biases in treadmill's force-plate data and exoskeletons' accelerometer data). These labeling inaccuracies, together with sensor noise and position drift inherent in the wearable soft sensors, naturally introduce realistic noise into the training data. Thus, the results demonstrate that the proposed framework is inherently robust to such real-world noise without requiring additional synthetic augmentation.

4) Comparison on Generalization After Fine-Tuning Across Subjects and Locomotion Modes: Table I reports estimation accuracy for each unseen subject in a leave-one-subject-out cross-validation setup, where the model is trained on data from the remaining eight subjects. Table II presents the performance for each locomotion mode, aggregated over all nine held-out test subjects. All results are obtained under Scenario (S3). These per-subject and per-mode breakdowns reveal variations in estimation performance not captured by aggregate metrics shown earlier.

Each estimation approach shows strengths under specific conditions. From Tables I and II, MAML consistently outperforms all baselines on average, across subjects and locomotion modes. Meanwhile, each baseline shows strengths suited to particular aspects of estimation: (a) TL performs comparably to MAML in gait phase classification across all subjects and locomotion modes, suggesting that its frozen feature extractor captures generalizable temporal gait patterns, while its trainable head adapts to subject-specific nuances. (b) SFT yields the lowest incline RMSE for most subjects (except Sub04, Sub06, and Sub07) and for most locomotion modes (except SA and SD), indicating that full-network fine-tuning is advantageous for capturing subtle, terrain-specific features important to incline estimation. (c) RI, though generally less accurate, performs strongly in locomotion mode classification, which is consistent with findings in Section IV-E.1 that training from scratch is effective for this high-level categorical estimation problem under sufficient calibration data.

MAML mitigates the effects of data imbalance. In our experiments, treadmill walking trials provide more data than stair climbing trials, resulting in data imbalance. Likely due to this imbalance, DE, TL, and SFT, which rely on standard supervised learning, exhibit elevated errors in stair scenarios (SA and SD) compared to treadmill walking (LW, RA, and RD). In contrast, MAML maintains robust performance across these scenarios, thanks to the adaptive meta-learning.

V. Conclusion and Future Work

This paper introduced an adaptive gait phase and terrain geometry estimation framework based on model-agnostic meta-learning (MAML) using a small set of wearable soft sensors. The estimation task was formulated as joint classification of gait phase and locomotion mode and regression of terrain incline angle. A multi-head deep convolutional neural network served as the framework's backbone, enabling shared feature extraction and simultaneous prediction of all estimation variables. Through MAML-based training, the model learns a subject- and terrain-invariant initialization that supports efficient fine-tuning with limited calibration data and strong generalization to previously unseen users and conditions.

While the proposed framework enables efficient adaptation with only a small amount of labeled calibration data, it still relies on supervised fine-tuning for user-specific adaptation. Eliminating the need for labeled calibration data is an important direction for future work. Unsupervised or self-supervised adaptation strategies, such as pseudo-label refinement, may offer a promising pathway toward label-free deployment [32]. Nevertheless, experimental results across nine subjects and five terrain conditions demonstrated that the proposed framework consistently outperforms conventional supervised and transfer learning baselines in estimation accuracy, adaptation efficiency, and generalization performance. Looking ahead, the proposed framework also paves the way for downstream applications such as exoskeleton control using wearable soft sensors, where accurate estimation of gait phase, locomotion mode, and terrain inclination is critical.

References

[1] A. J. Young and D. P. Ferris, "State of the art and future directions for lower limb robotic exoskeletons," *IEEE Trans. Neural Syst. Rehabil. Eng.*, vol. 25, no. 2, pp. 171–182, Feb. 2017.

[2] S. Luo et al., "Experiment-free exoskeleton assistance via learning in simulation," *Nature*, vol. 630, no. 8016, pp. 353–359, 2024.

[3] R. J. Cortino, T. K. Best, and R. D. Gregg, "Data-driven phase-based control of a powered knee-ankle prosthesis for variable-incline stair ascent and descent," *IEEE Trans. Med. Robot. Bionics*, vol. 6, no. 1, pp. 175–188, Feb. 2024.

[4] P. T. Chinimilli, Z. Qiao, S. M. R. Sorkhabadi, V. Jhawar, I. H. Fong, and W. Zhang, "Automatic virtual impedance adaptation of a knee exoskeleton for personalized walking assistance," *Robot. Auton. Syst.*, vol. 114, pp. 66–76, 2019.

[5] R. R. Posh and R. D. Gregg, "A task-agnostic approach to unified multi-activity gait phase estimation via bilateral sensing," in *Proc. Int. Conf. Rehabil. Robot*., 2025, pp. 1–8.

[6] S. Cheng, C. A. Laubscher, T. K. Best, and R. D. Gregg, "Ambilateral activity recognition and continuous adaptation with a powered knee-ankle prosthesis," *IEEE Trans. Robot.*, vol. 41, pp. 2251–2267, 2025.

[7] L. Alzubaidi et al., "Review of deep learning: Concepts, CNN architectures, challenges, applications, future directions," *J. Big Data*, vol. 8, no. 1, 2021, Art. no. 53.

[8] X. Hou and J. Bergmann, "Pedestrian dead reckoning with wearable sensors: A systematic review," *IEEE Sensors J.*, vol. 21, no. 1, pp. 143–152, Jan. 2021.

[9] Q. Yuan and I.-M. Chen, "3-D localization of human based on an inertial capture system," *IEEE Trans. Robot.*, vol. 29, no. 3, pp. 806–812, Jun. 2013.

[10] Y. Zhang, K. Chen, J. Yi, T. Liu, and Q. Pan, "Whole-body pose estimation in human bicycle riding using a small set of wearable sensors," *IEEE/ASME Trans. Mechatron.*, vol. 21, no. 1, pp. 163–174, Feb. 2016.

[11] D. Kim, J. Kwon, S. Han, Y.-L. Park, and S. Jo, "Deep full-body motion network for a soft wearable motion sensing suit," *IEEE/ASME Trans. Mechatron.*, vol. 24, no. 1, pp. 56–66, Feb. 2019.

[12] X. Li et al., "A shortcut enhanced LSTM-GCN network for multi-sensor based human motion tracking," *IEEE Trans. Autom. Sci. Eng.*, vol. 21, no. 4, pp. 5078–5087, Oct. 2024.

[13] D. D. Molinaro, K. L. Scherpereel, E. B. Schonhaut, G. Evangelopoulos, M. K. Shepherd, and A. J. Young, "Task-agnostic exoskeleton control via biological joint moment estimation," *Nature*, vol. 635, no. 8038, pp. 337–344, 2024.

[14] J. Xu et al., "Reciprocal learning of intent inferral with augmented visual feedback for stroke," in *Proc. Int. Conf. Rehabil. Robot.*, 2025, pp. 1512–1517.

[15] D. B. Kowalsky, J. R. Rebula, L. V. Ojeda, P. G. Adamczyk, and A. D. Kuo, "Human walking in the real world: Interactions between terrain type, gait parameters, and energy expenditure," *PLoS One*, vol. 16, no. 1, 2021, Art. no. e0228682.

[16] J. Xu et al., "ChatEMG: Synthetic data generation to control a robotic hand orthosis for stroke," *IEEE Robot. Automat. Lett.*, vol. 10, no. 2, pp. 907–914, Feb. 2025.

[17] D. Le, S. Cheng, R. D. Gregg, and M. Ghaffari, "Transfer learning for efficient intent prediction in lower-limb prosthetics: A strategy for limited datasets," *IEEE Robot. Automat. Lett.*, vol. 9, no. 5, pp. 4321–4328, May 2024.

[18] T. Hospedales, A. Antoniou, P. Micaelli, and A. Storkey, "Meta-learning in neural networks: A survey," *IEEE Trans. Pattern Anal. Mach. Intell.*, vol. 44, no. 9, pp. 5149–5169, Sep. 2022.

[19] W. Cao et al., "A fusion network with stacked denoise autoencoder and meta learning for lateral walking gait phase recognition and multi-step-ahead prediction," *IEEE J. Biomed. Health Inform.*, vol. 29, no. 1, pp. 68–80, Jan. 2025.

[20] P. L. La Rotta et al., "Meta-learning for fast adaptation in intent inferral on a robotic hand orthosis for stroke," in *Proc. IEEE/RSJ Int. Conf. Intel. Robot. Syst*., 2024, pp. 4693–4700.

[21] Z. Zhu, S. M. R. Sorkhabadi, Y. Gu, and W. Zhang, "Design and evaluation of an invariant extended Kalman filter for trunk motion estimation with sensor misalignment," *IEEE/ASME Trans. Mechatron.*, vol. 27, no. 4, pp. 2158–2167, Aug. 2022.

[22] J. K. Leestma, P. R. Golyski, C. R. Smith, G. S. Sawicki, and A. J. Young, "Linking whole-body angular momentum and step placement during perturbed human walking," *J. Exp. Biol.*, vol. 226, no. 6, 2023, Art. no. jeb244760.

[23] Y. Mengüç et al., "Wearable soft sensing suit for human gait measurement," *Int. J. Robot. Res.*, vol. 33, no. 14, pp. 1748–1764, 2014.

[24] L. Sanchez-Botero, A. Agrawala, and R. Kramer-Bottiglio, "Stretchable, breathable, and washable fabric sensor for human motion monitoring," *Adv. Mater. Technol.*, vol. 2023, Art. no. 2300378.

[25] J. C. Case, M. C. Yuen, J. Jacobs, and R. Kramer-Bottiglio, "Robotic skins that learn to control passive structures," *IEEE Robot. Automat. Lett.*, vol. 4, no. 3, pp. 2485–2492, Jul. 2019.

[26] W. Zhang et al., "Intelligent knee sleeves: A real-time multimodal dataset for 3D lower body motion estimation using smart textile," in *Proc. Int. Conf. Neural Inf. Process. Syst.*, 2023, pp. 42502–42515.

[27] A. Kharb, V. Saini, Y. Jain, and S. Dhiman, "A review of gait cycle and its parameters," *Int. J. Comput. Eng. Manag.*, vol. 13, no. 1, pp. 78–83, 2011.

[28] L. M. Mooney, E. J. Rouse, and H. M. Herr, "Autonomous exoskeleton reduces metabolic cost of human walking during load carriage," *J. Neuro-Engineering Rehabil.*, vol. 11, no. 1, 2014, Art. no. 80.

[29] C. Finn, P. Abbeel, and S. Levine, "Model-agnostic meta-learning for fast adaptation of deep networks," in *Proc. Int. Conf. Mach. Learn.*, 2017, pp. 1126–1135.

[30] D. P. Kingma and J. Ba, "Adam: A method for stochastic optimization," 2014, *arXiv:1412.6980*.

[31] F. Nogueira, "Bayesian optimization: Open source constrained global optimization tool for python," 2014. [Online]. Available: https://github.com/bayesian-optimization/BayesianOptimization

[32] K. Hsu, S. Levine, and C. Finn, "Unsupervised learning via meta-learning," in *Int. Conf. Learn. Represent.*, 2019.